Letter

Traveling pulses in type-I excitable media

Andreu Arinyo-i-Prats,[1,2] Pablo Moreno-Spiegelberg,[1] Manuel A. Matias,[1] and Damià Gomila[1,*]
[1]*IFISC (CSIC-UIB), Instituto de Física Interdisciplinar y Sistemas Complejos, E-07122 Palma de Mallorca, Spain*
[2]*Institute of Computer Science, Czech Academy of Sciences, 182 07 Praha 8, Czech Republic*

(Received 4 January 2021; accepted 28 October 2021; published 22 November 2021)

We consider a general model exhibiting type-I excitability mediated by a homoclinic and a saddle node on the invariant circle bifurcations. We show how the distinct properties of type-I with respect to type-II excitability confer unique features to traveling pulses in excitable media. They inherit the characteristic divergence of type-I excitable trajectories at threshold exhibiting analogous scalings in the spatial thickness of the pulses. Our results pave the way to identify basic underlying mechanisms behind type-I excitable pulses based solely on the characteristics of the pulse.

DOI: 10.1103/PhysRevE.104.L052203

Excitable media are spatially extended, nonequilibrium systems that account for the propagation of local excitable excursions. They are pervasive in nature with relevance in multiple fields, such as neuroscience [1], depression waves [2], cardiac tissue [3], reaction-diffusion systems [4–6], and nonlinear optics [7]. In excitable media, local perturbations may lead to a wide variety of spatial structures and patterns, such as waves, pulses, and spirals [4,5,8,9] (Fig. 1).

Many of the dynamical properties of excitable systems can be traced back to the kind of excitability (type-I or type-II) they display. The type of excitability is defined by the bifurcations delimiting the excitable region in parameter space. This distinction was clearly established in electric signals propagating in neurons in the form of spikes or pulses showing a different kind of responses to electric stimuli. The link between bifurcations and different types of excitable behavior in axons was first shown in Ref. [11], and how the bifurcations define the type of excitability is clearly defined in [12–14].

From a dynamical systems point of view, type-I excitability is mediated by either a saddle node on invariant cycle (SNIC) or a homoclinic bifurcation. In this scenario, there is a periodic orbit, related to the connection between a stable manifold of a stable node and the unstable manifold of a saddle, whose remnants after it is destroyed generate the excitable excursion. By contrast, type II is in general associated with the presence of a single stable focus and mediated by an Andronov-Hopf bifurcation where the cycle acquires, typically due to a slow-fast separation of timescales, a very large amplitude just after the bifurcation [15]. In this case, excitability is caused by resonant perturbations causing nonlinear amplifications of the input [13].

Despite the relation between excitable behavior and underlying bifurcations, excitable media are often studied in the framework of reaction-diffusion systems, without focusing on the excitability type. As discussed in this Letter, the type of excitability imprints unique features to traveling pulses, and such connection have been largely unexplored. Studies of excitable media often tend to use the microscale understanding of the system to propose dynamical models, such as in the case of the classical Belousov-Zhabotinskii reaction [16]. These models are most often placed in the range that shows type-II characteristics [5,8,17]. However, just recently, several works in the context of vegetation dynamics have suggested models that are better understood in the light of type-I excitable media [18–21]. In contrast to the widely explored spatiotemporal type-II excitability mechanism [7,22,23], there is only a partial understanding of the dynamical properties of spatial models showing type-I excitability [1,24,25].

In this Letter, we aim to address this open question characterizing propagating pulses in type-I excitable media. As our results show, important features of the spatiotemporal dynamics, such as the shape or length of the pulses, can be understood in the light of the excitable excursions of the temporal system mediated by bifurcations generating type-I behavior.

To approach this problem, we consider a normal form of codimension-3, which is the simplest model to describe both scenarios of type-I excitability [26], and to which we add one-dimensional (1D) diffusion to study spatial propagation,

$$\partial_t u = v + D\partial_{xx} u,$$
$$\partial_t v = \varepsilon_1 u^3 + \mu_2 u + \mu_1 + v(\nu + bu + \varepsilon_2 u^2) + D\partial_{xx} v. \quad (1)$$

We choose $\varepsilon_1 = \varepsilon_2 = -1$, which is the case that gives a complete description of type-I excitability. The spatial coupling is chosen diagonal and with the same strength in both equations to avoid additional effects such as Turing instabilities. Without loss of generality, the diffusion coefficient is fixed to one ($D = 1$). The resulting system describes, excluding particular diffusion couplings, any type-I system with a temporal part analogous to the normal form presented in Ref. [26]. Finally, we have fixed the parameters $\nu = 1$ and $b = 2.4$, considering μ_1 and μ_2 as our main control parameters. Here, $u(x,t)$ and $v(x,t)$ are real fields.

We first consider the temporal system ($D = 0$), which also describes the dynamics of the homogeneous solutions [$\partial_{xx} u = \partial_{xx} v = 0$ in (1)]. In particular, we focus on a parameter region in the neighborhood of a saddle-node separatrix

*damia@ifisc.uib-csic.es

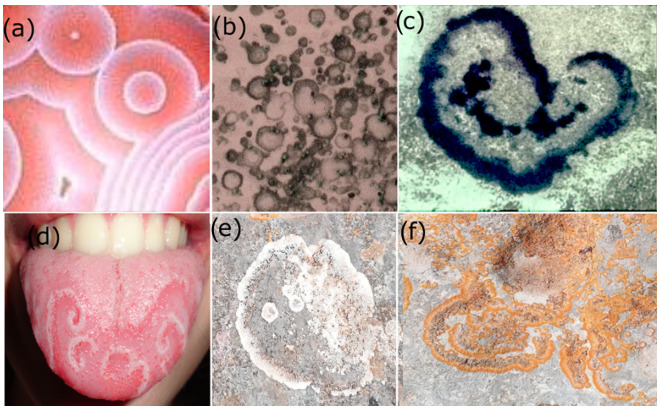

FIG. 1. Examples of traveling pulses in excitable media. (a) Waves in a Belousov-Zhabotinsky chemical reaction. (b) Rings of vegetation growing radially in intertidal salt marshes in Nanhui shoal, Shanghai. (c) Spiral formed by a seagrass traveling pulse in the coast of Mallorca in the Mediterranean Sea, Spain. (d) Geographic tongue caused by fungiform papillae, adapted from Ref. [10]. (e), (f) Two kinds of Rhizocarpon lichen in rocks, Mallorca. (a) and (d) are modeled as type-II excitable media, while (b) and (c) fit within the type-I framework. The excitable type of (e) and (f) has not yet been identified.

loop (SNSL) codimension-2 point of the temporal system, from which the two bifurcations of relevance—homoclinic and SNIC—eliciting type-I excitability emerge (Fig. 2). This two bifurcations mediate two different ways of entering the type-I excitable region marked by the label "c" [27,28]. This will have a direct effect on the behavior of the pulses to be considered below. Figures 2(a)–2(c) show a sketch of the phase space of the temporal system in each of the corresponding regions. In Fig. 2(a), the system has a limit cycle and an unstable focus. In Fig. 2(b), a limit cycle is around the three fixed points: node (P_1), saddle (P_2), and unstable focus (P_3), corresponding to the three homogeneous solutions of (1). In Fig. 2(c), the cycle has been destroyed either by the homoclinic or SNIC bifurcations leading to a type-I excitable regime.

We turn now to the spatiotemporal dynamics. In the excitable region, by initializing the system with a strong enough localized perturbation around the lower homogeneous solution, P_1, a pair of solitary (or traveling) pulses that propagate with fixed shape and constant and opposite velocities is generated. We take one of such pulses, i.e., the one moving to the left [Fig. 3(b)], to characterize in detail.

A convenient way to study these pulses is using a moving reference frame, $\xi = x - ct$, where c is the velocity of the pulse yet to be determined. In this coordinate system, the partial differential equations (1) become ordinary differential equations,

$$\begin{aligned} du/d\xi &= u_\xi, \\ dv/d\xi &= v_\xi, \\ du_\xi/d\xi &= -(v + c\,u_\xi), \\ dv_\xi/d\xi &= u^3 - \mu_2 u - \mu_1 - v(1 + bu - u^2) - c\,v_\xi. \end{aligned} \tag{2}$$

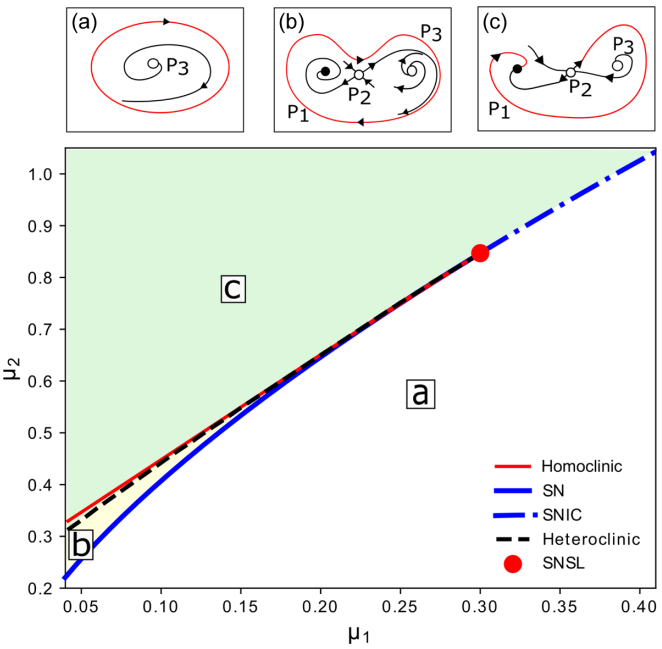

FIG. 2. Phase diagram of the system (1) including the bifurcation lines of homogeneous and traveling pulse solutions. The diagram is organized by a SNSL codimension-2 point (red dot) from which a SNIC (blue dot-dashed line) and homoclinic of a stable cycle (red line) bifurcation lines emerge for the temporal dynamics. The diagram is completed by the heteroclinic bifurcation line of traveling pulses (dashed black line). For the temporal system, excitable excursions occur in the area above the SNIC and homoclinic lines. For the spatiotemporal system, excitable traveling pulses can form in this green shaded area. The insets show a schematic representation of the phase space for the temporal system in each corresponding area. P_1, P_2, and P_3 indicate the fixed, saddle, and unstable fixed points, respectively, for each region, and the limit cycle and its remnants are shown as a red line.

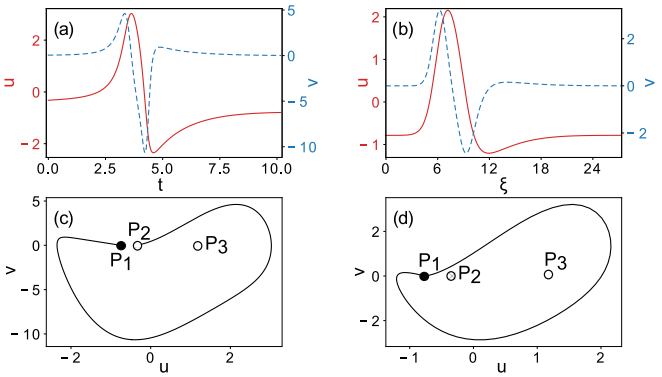

FIG. 3. Comparison of the temporal dynamics of an excitable excursion and the spatial profile of a 1D traveling pulse sustained by this excitable dynamics. (a) Temporal (spatially homogeneous) excitable trajectory of u (red solid line) and v (blue dashed line) starting from an initial condition just above the saddle point P_2. (b) Stable 1D traveling pulse as a function of the spatial coordinate ξ in the moving reference frame. (c),(d) The temporal excitable excursion and the traveling pulse in the (u, v) phase space, respectively. P_1, P_2, and P_3 indicate stable, saddle, and unstable fixed points. Here, $\mu_1 = 0.3$ and $\mu_2 = 1.0$.

Trajectories of this dynamical system describe stationary solutions of (1) in the reference frame moving with velocity c [29]. Only bounded trajectories have a physical meaning. In particular, excitable traveling pulses are represented in this system as homoclinic trajectories originating from the lower fixed point P_1 [Fig. 3(d)]. c is computed numerically simultaneously with the field profile using a Newton method [30], and it varies weakly with parameters in the excitable region.

Although the dynamical system describing temporal dynamics for homogeneous solutions (1) and the spatial dynamical system (2) are apparently very different, one observes important similarities in their solutions. Roughly speaking, a traveling pulse transcribes the temporal dynamics in space, such that the spatial profile of the pulse resembles the excitable trajectory in time. It is important to remark, however, that whereas excitable temporal (homogeneous) trajectories are open, the spatial pulses show a closed trajectory in phase space [compare Figs. 3(a), 3(c) and Figs. 3(b), 3(d)]. This transcription of the dynamics also occurs in the type-II case, where the excitable pulses inherit the square shape from the slow-fast feature of the temporal trajectories (see, for instance, Fig. 3.2 in Ref. [5]). We would like to emphasize the difference in the shape between both types of excitable media.

The similarity between the temporal and spatial trajectories anticipates the results that follow.

We next study how the two different bifurcations leading to type-I excitability in the temporal system, i.e., the homoclinic and SNIC bifurcations, shape the excitable pulses. To do so, we study the stability of traveling pulses in the (μ_1, μ_2) parameter space [31]. Traveling pulses are stable in the part of the excitable region "c" shown in Fig. 2, and are destroyed at the SNIC or at the heteroclinic bifurcation, as indicated with a black dashed line in Fig. 2. The homoclinic and SNIC bifurcations of the temporal systems are directly related to the heteroclinic and SNIC bifurcations of the traveling pulses.

Let us first consider the heteroclinic curve (black dashed line in Fig. 2). Close to the bifurcation in parameter space, the pulse shape changes drastically, generating a plateau at the value of the middle (saddle, P_2) homogeneous solution [Fig. 4(b)]. As the spatial trajectory is closer to the saddle point (through its stable manifold), there is a slowing down of the spatial dynamics, inherited from the temporal homoclinic [Fig. 4(a)], that manifests as a plateau in the spatial profile. The plateau enlarges as the parameters are close to the bifurcation (black dashed line), diverging at the threshold. Figure 4(c) shows instead the temporal excitable excursion in the (u, v) phase space, where the trajectory approaches the saddle point P_2. The spatial counterpart [Fig. 4(d)] behaves analogously, leading to the formation of a double heteroclinic at threshold, where the size of the plateau diverges. Such bifurcation has been studied in [24,32] in relation to a T-point of the spatial dynamics, but the connection with the homoclinic bifurcation of the temporal systems was not considered. Strictly speaking, in a finite-size system, this divergence cannot be observed, but the bifurcation will manifest as a fold of the traveling pulse [24].

This slowing down has a characteristic logarithmic scaling law in the width of the plateau with respect to the parameter distance to the bifurcation [33], which is captured by the obtained solutions, as shown in Fig. 6(a). The red line indicates the expected scaling slope from theory, which depends on the logarithmic parameter distance divided by the (independently obtained) leading unstable spatial eigenvalue of the saddle point, and we can see that the agreement is perfect.

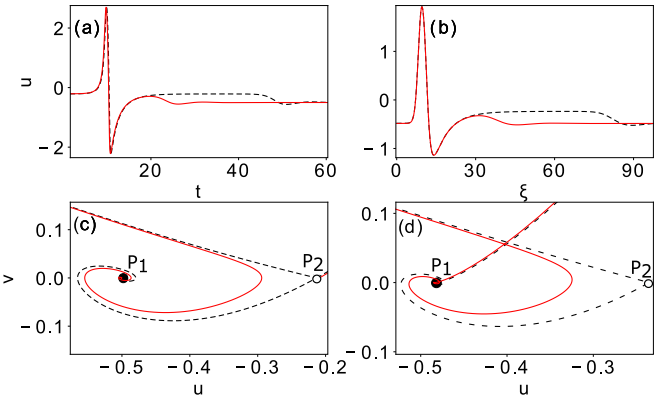

FIG. 4. (a) Divergence of the duration of the excitable excursion in the temporal system approaching the homoclinic bifurcation, and (b) divergence of the plateau in the pulses approaching the heteroclinic bifurcation. Here, $\mu_2 = 0.4$ and $\mu_1 = \mu_{1c} - \Delta\mu_1$, where the homoclinic bifurcation occurs at $\mu_{1c} = 0.075\,603\,955\,87$ for the temporal system, and the heteroclinic bifurcation occurs at $\mu_{1c} = 0.081\,078\,760\,02$ for the spatial system, and $\Delta\mu_1 = 10^{-3}$ (red solid line) and $\Delta\mu_1 = 10^{-12}$ (black dashed line). In all panels, P_1, P_2 signal the stable and saddle fixed points, respectively. (c), (d) A zoom of the most relevant region in the phase space (u, v) for the temporal and spatial dynamics.

The fact that the heteroclinic bifurcation curve closely follows the homoclinic line of the temporal system (Fig. 2), and that the width of a traveling pulse follows the same scaling as the duration of a temporal pulse, indicate how the bifurcations of the temporal dynamics permeate the spatial dynamical description of traveling pulses, even though the connection is not straightforward from the equations.

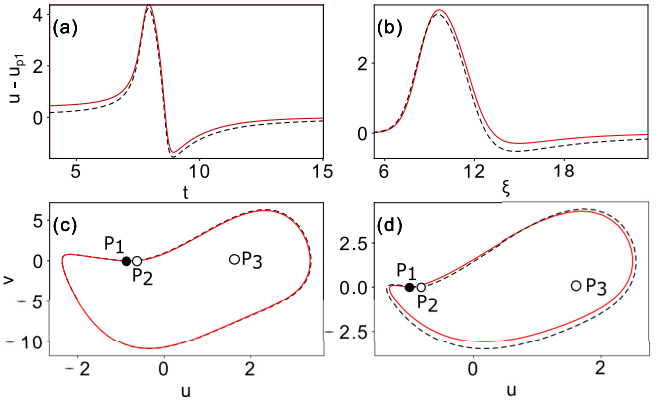

FIG. 5. Same as in Fig. 4 for the SNIC bifurcation. $u - u_{P_1}$ is plotted in (a) and (b), where u_{P_1} is the value of u at the stable fixed point P_1. Here, $\mu_2 = 2.0$ and $\mu_{1c} = 1.0887$ with $\Delta\mu_1 = -10^{-4}$ and $\Delta\mu_1 = -10^{-1}$ for the black dashed and red solid curves, respectively. (c), (d) The phase space (u, v) for the temporal and spatial dynamics, respectively.

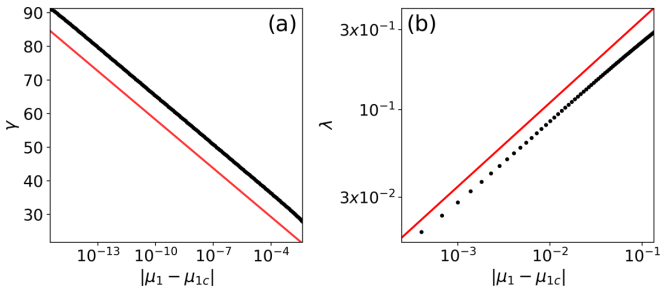

FIG. 6. (a) Scaling of the pulse width, γ, approaching the heteroclinic bifurcation. γ is defined as the distance from where the pulse separates 10^{-2} from the stable homogeneous solution until it comes back to the same distance (black points). The expected scaling is $\gamma = \frac{1}{\lambda_1}\ln(|\mu_1 - \mu_{1c}|)$ (red line in the plot), where λ_1 is the closest eigenvalue to zero of the saddle point in the spatial dynamics. (b) Scaling of the rate λ at which the tail of the traveling pulse exponentially approaches the saddle, as a function of the parameter distance to the SNIC bifurcation. The expected scaling is a power law with exponent $1/2$: $\lambda \propto \sqrt{|\mu_1 - \mu_{1c}|}$ (red line).

Next we analyze what happens to the pulse at the SNIC bifurcation [34]. Beyond the SNIC bifurcation (blue dash-dotted line in Fig. 2), a temporal cycle is reconstructed when the saddle P_2 and the node P_1 collide. As parameters are set closer to the SNIC from the excitable region, the trajectories triggered by perturbations need more time to return to the stable fixed point P_1, as its eigenvalue tends to zero. As a result, the tail behind the traveling pulses also gets longer and longer [Fig. 5(d)].

For the SNIC in the temporal case, the power law manifests in the divergence of the characteristic time to reach the stable fixed point [28]. Analogously, one would expect that the pulse thickness scales as a power law that diverges at the onset of bifurcation. However, due to the exponential approach to the saddle close to the bifurcation, the thickness of the pulse is not well defined. Therefore, we have turned to measure the approach rate that is proportional to the leading spatial eigenvalue, which becomes zero at the bifurcation. This scaling is shown in Fig. 6(b) and, as expected in a saddle-node bifurcation, it follows a power law with exponent $1/2$. The behavior of the system at the other side of the bifurcation corresponds to a wave train, which in this case is the analog of a temporal periodic behavior, with the SNIC marking a transition from wave trains to pulses.

In this Letter, we have shown the existence of 1D traveling pulses in a general model for type-I excitable media. Most studies in the literature of propagating structures in excitable media correspond to type-II excitability, found, e.g., in reaction-diffusion systems and the heart. On the other hand, an increasing number of studies report type-I excitable structures [18–21,25], although these structures have not been characterized yet. Still, they exhibit some distinctive features when comparing with type-II excitable pulses, such as their shapes, that are square in the latter case and smoother in the case of type-I excitable pulses. This difference between the pulse shaped, already obvious when comparing the excitable trajectory in temporal systems, is not casual, but a direct consequence of the mechanisms behind the excitability. The typical squared shape of type-II pulses arises from two very different (slow-fast) timescales, a key ingredient of this kind of excitability. A type-I excitable system, on the other hand, does not need such difference of timescales, which makes its shape smoother.

In our study, we have used a model that exhibits two routes corresponding to type-I excitability, mediated by two different bifurcations, i.e., SNIC and homoclinic (saddle loop), and we find key similarities between the temporal dynamics and the spatial profile of traveling pulses. In particular, type-I traveling pulses exhibit the same scaling behaviors for their width as those found in the duration of the excitable excursions in the temporal case, namely, logarithmic for the heteroclinic and power law for the SNIC bifurcations, respectively. This equivalency in the scaling behaviors unveils a nontrivial relation between temporal systems and the spatiotemporal structures of partial differential equations. Such general properties related to the type of excitability could be used to identify the dynamical mechanisms behind traveling pulses from empirical evidence. Other instabilities of traveling pulses in this system will be studied elsewhere [35].

Grants RTI2018-095441-B-C22 and MDM-2017-0711 funded by MCIN/AEI/10.13039/501100011033 and by ERDF A way of making Europe. We acknowledge helpful discussions with A. Pérez-Cervera.

A.A-i-P. and P.M-S. contributed equally to this work.

[1] R. Follmann, E. Rosa, Jr., and W. Stein, Phys. Rev. E **92**, 032707 (2015).
[2] M. A. Dahlem and S. C. Müller, Ann. Phys. **13**, 442 (2004).
[3] V. S. Zykov, Ann. N.Y. Acad. Sci. **591**, 75 (1990).
[4] E. Meron, Phys. Rep. **218**, 1 (1992).
[5] A. S. Mikhailov, *Foundations of Synergetics. I. Distributed Active Systems* (Springer, Berlin, 1990).
[6] K.-J. Lee, W. D. McCormick, J. E. Pearson, and H. L. Swinney, Nature (London) **369**, 215 (1994).
[7] F. Marino and S. Balle, Phys. Rev. Lett. **94**, 094101 (2005).
[8] *Chemical Waves and Patterns*, edited by R. Kapral and K. Showalter (Kluwer Academic, Dordrecht, 1995).
[9] S. Alonso, M. Bär, and B. Echebarria, Rep. Prog. Phys. **79**, 096601 (2016).
[10] https://commons.wikimedia.org/wiki/File:Geographic_tongue.JPG.
[11] J. Rinzel and G. B. Ermentrout, in *Methods in Neuronal Modeling: From Synapses to Networks*, edited by C. Koch and I. Segev (MIT Press, Cambridge, 1989), pp. 135–169.
[12] E. M. Izhikevich, *Dynamical Systems in Neuroscience* (MIT Press, Cambridge, 2007).
[13] E. M. Izhikevich, Intl. J. Bif. Chaos **10**, 1171 (2000).
[14] Z. Zhao and H. Gu, Sci. Rep. **7**, 1 (2017).

[15] A saddle node (off the invariant cycle) can also originate type-II excitability in some cases [14].
[16] J. Hudson and J. Mankin, J. Chem. Phys. **74**, 6171 (1981).
[17] J. Keener and J. Sneyd, *Mathematical Physiology* (Springer, New York, 1998).
[18] D. Ruiz-Reynés, D. Gomila, T. Sintes, E. Hernández-García, N. Marbà, and C. M. Duarte, Sci. Adv. **3**, e1603262 (2017).
[19] C. Fernandez-Oto, D. Escaff, and J. Cisternas, Ecol. Complex. **37**, 38 (2019).
[20] A. Iuorio and F. Veerman, Physica D **427**, 133015 (2021).
[21] L.-X. Zhao, K. Zhang, K. Siteur, X.-Z. Li, Q.-X. Liu, and J. van de Koppel, Sci. Adv. **7**, eabe1100 (2021).
[22] S. Beri, L. Mashall, L. Gelens, G. Van der Sande, G. Mezosi, M. Sorel, J. Danckaert, and G. Verschaffelt, Phys. Lett. A **374**, 739 (2010).
[23] M. K. McGuire, C. A. Fuller, J. F. Lindner, and N. Manz, Chaos **31**, 033118 (2021).
[24] M. Or-Guil, J. Krishnan, I. G. Kevrekidis, and M. Bär, Phys. Rev. E **64**, 046212 (2001).
[25] K. Alfaro-Bittner, S. Barbay, and M. Clerc, Chaos **30**, 083136 (2020).
[26] F. Dumortier, R. Roussarie, J. Sotomayor, and H. Zoladek, *Bifurcations of Planar Vector Fields: Nilpotent Singularities and Abelian Integrals* (Springer, Berlin, 2006).
[27] P. Gaspard, J. Phys. Chem. **94**, 1 (1990).
[28] A. Jacobo, D. Gomila, M. A. Matías, and P. Colet, Phys. Rev. A **78**, 053821 (2008).
[29] O. Jaïbi, A. Doelman, M. Chirilus-Bruckner, and E. Meron, Physica D **412**, 132637 (2020).
[30] A. Scroggie, D. Gomila, W. Firth, and G.-L. Oppo, Appl. Phys. B **81**, 963 (2005).
[31] This is the stability of traveling pulses if determined computing the eigenvalues of the Jacobian of Eq. (1) using the stationary solutions obtained in the moving reference frame with a Newton-Raphson method.
[32] B. Sandstede and A. Scheel, Nonlinearity **13**, 1465 (2000).
[33] The logarithmic scaling law in the spatial coordinate ξ is analogous to the temporal logarithmic scaling of the homoclinic (saddle-loop) bifurcation [27]. As shown in the caption of Fig. 4 and in Fig. 6, such logarithmic scaling requires a very high accuracy in the determination of the threshold to clearly observe the divergence approaching the bifurcation.
[34] In the spatial dynamical system, the traveling pulse is technically destroyed at a SNSL bifurcation. This bifurcation occurs for the same parameters as the SNIC in the temporal system [35].
[35] P. Moreno-Spiegelberg *et al.*, Bifurcation structure of traveling pulses in type-I excitable media (unpublished).